UNIVERSITY OF HELSINKI

https://helda.helsinki.fi

Purine availability determines survival of complex I-deficient fibroblasts under OXPHOS-reliant condition

Ermert, Melisa Emel; Pennings, Bas; Perkovic, Anja; Pecheritsyna, Svetlana; Schomakers, Bauke ...

2027-01
Elsevier B.V.
http://hdl.handle.net/10138/640535
Ermert, M E, Pennings, B, Perkovic, A, Pecheritsyna, S, Schomakers, B, van Weeghel, M, Smeitink, J, Houtkooper, R, Pirinen, E & Renkema, H 2027, 'Purine availability determines survival of complex I-deficient fibroblasts under OXPHOS-reliant condition', Mitochondrion, vol. 92, 102223. https://doi.org/10.1016/j.mito.2026.102223

Downloaded from Helda, University of Helsinki institutional repository. https://helda.helsinki.fi
This is an electronic reprint of the original article.
This reprint may differ from the original in pagination and typographic detail.
Please cite the original version.

Mitochondrion 92 (2027) 102223

Contents lists available at ScienceDirect

Mitochondrion

journal homepage: www.elsevier.com/locate/mito

Purine availability determines survival of complex I-deficient fibroblasts under OXPHOS-reliant condition

Melisa Emel Ermert [a,b,c], Bas Pennings [a], Anja Perkovic [a], Svetlana Pecheritsyna [a], Bauke Schomakers [b,d], Michel van Weeghel [b,c,d,e], Jan Smeitink [a], Riekelt Houtkooper [b,c,e,f], Eija Pirinen [g,h,i,j], Herma Renkema [a,*]

[a] Khondrion B.V. Nijmegen, the Netherlands
[b] Laboratory Genetic Metabolic Diseases, Amsterdam UMC location University of Amsterdam, Meibergdreef 9, 1105, AZ, Amsterdam, the Netherlands
[c] Amsterdam Gastroenterology, Endocrinology and Metabolism Institute, Amsterdam UMC, Amsterdam, the Netherlands
[d] Core Facility Metabolomics, Amsterdam UMC Location University of Amsterdam, Meibergdreef 9, Amsterdam, the Netherlands
[e] Amsterdam Cardiovascular Sciences institute, Amsterdam, the Netherlands
[f] Emma Center for Personalized Medicine, Amsterdam UMC, Amsterdam, the Netherlands
[g] Research Unit of Biomedicine and Internal Medicine, Faculty of Medicine University of Oulu, 90014 Oulu, Finland
[h] Research Program for Clinical and Molecular Metabolism, Faculty of Medicine, University of Helsinki, Helsinki, Finland
[i] Medical Research Center Oulu, Oulu University Hospital and University of Oulu, Oulu, Finland.
[j] Biocenter Oulu, Faculty of Medicine, University of Oulu, Oulu, Finland

ARTICLE INFO

Keywords:
Purine metabolism
NAD^+ homeostasis
Galactose medium
Complex-I deficiency
Primary mitochondrial disease

ABSTRACT

Growing fibroblasts in medium containing galactose instead of glucose makes cells more dependent on oxidative phosphorylation (OXPHOS) rather than glycolysis. Recently, it has been shown that treatment with nicotinamide adenine dinucleotide (NAD^+) improves cell viability of human OXPHOS Complex I-deficient skin fibroblasts in this OXPHOS-reliant condition. To study the effects of NAD^+ precursors in this model, we supplemented the cells with trigonelline (TG), nicotinamide (NAM), nicotinamide riboside (NR), nicotinamide mononucleotide (NMN) and found no improvement in cell viability, while supplementation with niacin (NA) did partially. Interestingly, cell viability was improved by addition of the NAD^+ building block adenosine monophosphate (AMP). Metabolic profiling showed a decrease in inosine monophosphate (IMP), a purine intermediate, under OXPHOS-reliant condition. Treatment with AMP and adenosine under this condition increased the IMP levels. Among nucleosides, only adenosine and guanosine treatments in OXPHOS-reliant condition improved the patient cell viability. Therefore, we conclude that OXPHOS-reliant condition limited purine nucleotide biosynthesis and salvage pathways, which could be overcome by increasing IMP levels. Together, our results reveal a previously unrecognized role for purine metabolism under OXPHOS-reliant condition, highlighting it as a candidate for therapeutic intervention.

1. Introduction

Primary mitochondrial diseases (PMD) are a group of hereditary metabolic disorders caused by pathogenic variants in the subunits of the OXPHOS complexes or their assembly factors, or proteins involved in mitochondrial DNA replication, mitochondrial translation, or mitochondrial dynamics, such as fusion and fission, directly affecting the function of the OXPHOS system(Chinnery, 2021). Treatments for PMD patients are mainly supportive, and approved treatment options are emerging for a few subtypes that only small patient subsets benefit

Abbreviations: AMP, adenosine 5′-monophosphate; cDNA, complementary DNA; CMP, cytidine 5′-monophosphate; GFP, green fluorescent protein; GMP, guanosine 5′-monophosphate; IMP, inosine 5′-monophosphate; NA, niacin; NAD^+, nicotinamide adenine dinucleotide; NADH, reduced nicotinamide adenine dinucleotide; $NADP^+$, nicotinamide adenine dinucleotide phosphate; NADPH, reduced nicotinamide adenine dinucleotide phosphate; NAM, nicotinamide; NMN, nicotinamide mononucleotide; NR, nicotinamide riboside; OXPHOS, oxidative phosphorylation; PMD, primary mitochondrial diseases; SAH, S-Adenosyl-L-homocysteine; SAM, S-adenosy-L-methionine; TG, trigonelline; UMP, uridine 5′-monophosphate; UDP, uridine diphosphate.

* Corresponding author.
E-mail address: renkema@khondrion.com (H. Renkema).

https://doi.org/10.1016/j.mito.2026.102223
Received 13 April 2026; Received in revised form 2 October 2026; Accepted 7 October 2026
Available online 8 October 2026
1567-7249/© 2026 The Authors. Published by Elsevier B.V. This is an open access article under the CC BY-NC-ND license (http://creativecommons.org/licenses/by-nc-nd/4.0/).

(Leber's hereditary optic neuropathy; Raxone(EPAR, 2015), Barth Syndrome; FORZINITY™(FDA, 2025), Thymidine kinase 2 deficiency; Kygevvi(EPAR, 2026)). The lack of approved drugs for mitochondrial dysfunction is partly due to the heterogeneous clinical presentations of patients, long diagnostic odyssey, and the lack of reliable treatment biomarkers(Zong et al., 2024). Although there are >300 genes known to differentially affect mitochondrial OXPHOS function, there may be common biochemical modalities that are affected, warranting more studies on the pathomechanisms of PMD.

Studying PMD with in vitro models is challenging because even in the presence of oxygen, cultured human skin fibroblasts are mainly glycolytic and reduce pyruvate to lactate rather than oxidize it to acetyl coenzyme A. This phenomenon is called the Crabtree effect in vitro cultured cells in general, similar to the Warburg effect, which is mainly observed in cancer cells(de Kok, 2021). Although there are different strategies to induce reliance on OXPHOS in cultured cells(de Kok, 2021) replacing glucose present in standard culture medium with its epimer, galactose, remains a fast and robust method(Robinson et al., 1992). Galactose is not a suitable source for glycolysis, as it first needs to be converted to glucose via the Leloir pathway, which occurs at a slow rate and consumes energy. Under this condition, patient cells with various OXPHOS defects were not viable(Robinson et al., 1992). This phenotypic difference between OXPHOS-deficient and healthy cells enables the testing of potential treatments that improve the viability of OXPHOS-deficient cells in this OXPHOS-reliant condition.

Given the urgent need for broadly applicable therapeutic strategies in PMD, molecules that support core mitochondrial metabolic functions, such as NAD^+, have emerged as particularly promising drug candidates. NAD^+ is an indispensable coenzyme composed of adenine- and nicotinamide-containing nucleotides joined by phosphate linkages (Nakamura et al., 2012). Direct NAD^+ supplementation has been shown to increase intracellular NAD^+ levels, restore redox balance, and improve the viability of Complex I-deficient patient fibroblasts in the OXPHOS-reliant condition(Iannetti et al., 2018). However, NAD^+ has limited bioavailability when administered orally, due to rapid degradation in circulation. Because of that, research focuses on NAD^+ precursors, given their superior clinical relevance due to their higher bioavailability and stability(Jianying Zhang et al., 2025).

NAD^+ is synthesized from its precursors, such as tryptophan or niacin, but predominantly it is recycled from NAM, NR, or NMN (Imai, 2018). TG is a methylated NA derivative proposed to enter the Preiss–Handler pathway to form NAD^+(Membrez et al., 2024). NAD^+ functions as a central electron carrier in the NAD^+/NADH and $NAD(P)^+$/NADPH redox couples. Because mitochondrial function relies on balanced $NAD(P)^+$/NAD(*P*)H pools, any alteration in NAD metabolite levels could impair mitochondrial processes. Upon Complex I (NADH: ubiquinone oxidoreductase) deficiency, NADH oxidation to NAD^+ is disrupted, leading to reductive stress(Xiao and Loscalzo, 2020), which cells can partially compensate for by converting pyruvate to lactate to regenerate NAD^+(Adant et al., 2022).

In this study, Complex I-deficient patient fibroblasts were treated with NAD^+ precursors to determine whether these compounds could reproduce the beneficial effect of NAD^+ under OXPHOS-reliant condition. Furthermore, we sought to identify the molecular pathway(s) through which NAD^+ improves the viability of Complex I-deficient cells under OXPHOS-reliant condition.

2. Materials and methods

2.1. Cell lines and cell culture

All primary human fibroblast cell lines from forearm skin biopsies of patients with nuclear Complex I subunit mutations and healthy controls used throughout this study were received from RadboudUMC, Nijmegen, the Netherlands, and informed consent from donors or patient's family members was obtained (relevant information is listed in Supplementary Table S1, including Complex I activities reported by (Koopman et al., 2007). Cells were maintained in M199 medium with HEPES and L-glutamine (#22340–087, Thermo Fisher Scientific) supplemented with 10% (*v*/v) Fetal Bovine Serum (FBS; #SV30160.03, Cytiva) and 100 IU/mL penicillin/streptomycin (P/S; #15140–122, Gibco) (complete M199 medium) in a humidified incubator with 5% CO_2 at 37 °C. Cells were passaged when they reached 80% subconfluency, and cell culture medium was refreshed once between passages.

2.2. Compound treatments

Compound treatments were prepared in Dulbecco's Modified Eagle Medium (DMEM; #A1443001, Thermo Fisher Scientific) supplemented with 2 mM L-alanyl-L-glutamine (GlutaMAX; #35050061, Thermo Fisher Scientific), 10% (*v*/v) dialyzed FBS; (#26400044, Thermo Fisher Scientific), 10 mM HEPES (#15630080, Thermo Fisher Scientific), 100 IU/mL P/S and 0.02 mM Phenol Red (#3532, Sigma-Aldrich) containing either 5.5 mM glucose (D(+)-Glucose; #1.08337.0250, Sigma-Aldrich) for the control condition, or 5.5 mM galactose (D(+)-Galactose; #G5388, Sigma-Aldrich). The paper refers to these as control or OXPHOS-reliant condition, respectively. Dialyzed FBS was used in both the glucose and galactose media throughout the study to reduce the glucose levels present in normal FBS that could contribute to cellular metabolism and interfere with the interpretation of the control (glucose media) versus OXPHOS-reliant (galactose media) condition comparison.

The following compounds were dissolved directly in control or OXPHOS condition to their final treatment concentrations: β-Nicotinamide Adenine Dinucleotide (NAD^+; #HY-B0445, MedChemExpress), Nicotinamide (NAM; #N3376, Sigma-Aldrich), β-Nicotinamide mononucleotide (NMN; #HY-F0004, MedChemExpress), Nicotinamide riboside chloride (NR; #HY-123033 A, MedChemExpress), Nicotinic acid (Niacin; N4126, Sigma-Aldrich), Trigonelline chloride (#HY-N0415, MedChemExpress), Sodium Pyruvate (#11360070, Gibco), adenosine 5′-monophosphate sodium salt (AMP; #A1752, Sigma-Aldrich), adenosine (#HY-B0228, MedChemExpress), guanosine (#HY-N0097, MedChemExpress), cytidine (#HY-B0158, MedChemExpress), uridine (#HY-B1449, MedChemExpress), adenine hemisulfate (#HY-B0152B, MedChemExpress), D-Ribose (#HY-W018772, MedChemExpress). Treatments were prepared fresh before each experiment.

2.3. Lentiviral complementation

Primary patient fibroblasts PT3 and PT4, and the control fibroblast CT1, were complemented by lentiviral infection using constructs that carry wild-type NDUFS7 subunit cDNA or GFP cDNA as described (Renkema et al., 2014).

2.4. Viability assay

Cells were detached by trypsinization (Trypsin-EDTA; #15400054, Gibco) and seeded to either clear flat-bottom (#655180, Greiner Bio-One) or black micro-clear bottom (#655090, Greiner Bio-One) 96-well plates at a seeding density of 4500 cells/well in complete M199 medium. After 24 h of incubation, medium was removed, and cells were washed 4 times with 200 μL/well basal medium (Glucose-free DMEM with HEPES, GlutaMAX, and P/S). After washing, 150 μL of treatment medium were added to each well and incubated for 72 h. After incubation, the cells were washed with 100 uL/well of M199 without phenol red (#11043023, Thermo Fisher Scientific) (wash medium). Then, 50 μL of 0.5 μM Calcein AM Viability Dye (#65–0853-39, Invitrogen) in wash medium was added. After 20 min of incubation in a humidified atmosphere with 5% CO_2 at 37 °C, the staining solution was removed, and wells were washed twice with 100 μL/well of wash medium. 100 μL/well of wash medium was added to the wells for fluorescence microscopy imaging with the BD Pathway 855 High-Content Bioimager (Becton Dickinson). Data from fluorescence microscopy pictures were

extracted as previously described by(Iannetti et al., 2016). Viability is quantified as the sum of the pixels with a calcein signal above the set fluorescence intensity threshold for each well. The contrasts of the fluorescence microscopy images were increased 5–10% for visualization purposes only; data analyses from the original '.tiff' files were conducted independently of signal intensity.

2.5. Lactate quantification

Extracellular lactate was quantified in 72-h post-treatment assay medium using an enzymatic cycling method adapted from (Schmiedeknecht et al., 2022). Briefly, the pyruvate to lactate conversion by L-lactate dehydrogenase (L-LDH; #10127230001, Roche) is linked to the iodonitrotetrazolium chloride (INT; #HY-15920, MedChemExpress) to formazan dye conversion by 1-Methoxyphenazine methosulfate (m-PMS; #HY-D0937, MedChemExpress). Assay buffer was prepared with 0.17 M Tris base pH 8.2 (#15504020, Invitrogen), 16.6 μM β-nicotinamide adenine dinucleotide, 4.95 μM INT, 34.7 pM L-LDH and 67.5 pM m-PMS. Sodium L-lactate (#L7022, Sigma-Aldrich) standards from 0.75 to 12 mM were prepared in control condition medium. 50 μL of sample/standard was mixed with 50 μL assay buffer in a clear 96-well assay plate. The assay plate was incubated for 1 h at room temperature in the dark. Thereafter, 50 μL 1 M acetic acid (#320099, Sigma-Aldrich) was added to the wells to stop the reaction. Absorbance was measured with the microplate reader at 490 nm and 650 nm. The latter was used as the reference and subtracted from the 490 nm absorbance values. Standard curve was generated using a second-order polynomial equation. To determine L-lactate concentration in the samples, their absorbance values were interpolated against the standard curve. Lactate was reported under control condition only, as it was undetectable in OXPHOS-reliant condition.

2.6. Intracellular NAD^+ and ATP measurement

To measure intracellular NAD^+ and ATP cells were plated and treated as described above. After 24 h, cells were washed 4 times with 200 μL per well of basal medium.

Intracellular NAD^+ was quantified using the NAD/NADH-Glo Assay (#G9071, Promega) according to manufacturer's protocol. Luminescence was recorded using the microplate plate reader (FLUOstar Omega, BMG Labtech) (30 cycles, 1 h). For the analysis, luminescence kinetic measurements were imported into GraphPad Prism software and area under the curve (AUC) was calculated for NAD^+ standards and experimental samples. NADH concentrations were below the reliable detection range, therefore not reported. From a total lysate volume of 50 μL, 20 μL was used for the NAD^+ quantification.

The remaining cell lysates (30 μL) were used to quantify intracellular ATP levels. For this, 30 μL ATP Lysis buffer containing 4 mM EDTA (#E4884, Sigma-Aldrich), 0,2% (*v*/v) Triton-X-100 (#X100, Sigma-Aldrich) in PBS was added to each well to obtain samples in ATP/DNA dilution buffer. 10 μL sample and 10 μL ATP (#11140965001, Sigma-Aldrich) standards (100–1000 nM in ATP/DNA dilution buffer) were transferred into a white flat bottom 96 well assay plate. 90 μL ATP Measurement Buffer containing 25 mM HEPES (#H3375, Sigma-Aldrich) pH 7.25, 0,3 mM D-Luciferin (#L2912, Thermo Fisher Scientific), 75 μM DTT (#43819, Sigma-Aldrich), 6.25 mM $MgCl_2$ (#76021126, Boom), 0,625 mM EDTA, 1 mg/mL BSA (#A9647, Sigma-Aldrich), 0.5 μg/mL Luciferase (#SRE0045, Sigma-Aldrich) in milliQ water was added to each well. The plate was incubated on ice in the dark for 10 min, and luminescence was recorded with a microplate reader. ATP standards were used to interpolate sample concentrations.

The remaining cell lysates (50 μL) from ATP measurement were used for Quant-iT PicoGreen dsDNA assay (#P-7589, Molecular Probes) DNA concentration quantification. Briefly, the plate with the lysates were freeze-thawed 3 times. Samples were diluted 2.5 times in ATP/DNA dilution buffer. 50 μL diluted samples and dsDNA standards (31.3–1000 ng/mL in ATP/DNA dilution buffer) were transferred to a black V-bottom 96-well assay plate (#651209, Greiner). 50 μL 200 times diluted PicoGreen solution in TE buffer was added to each well. After incubating 5 min at slow shaking speed on a plate shaker in the dark, fluorescence intensity was measured using the 1000 ng/mL DNA standard for gain adjustment. DNA standards were used to interpolate sample concentrations.

NAD^+ and ATP values for each sample were normalized to dsDNA concentrations. With this method, NAD^+, ATP, and dsDNA were measured from the same cell lysate.

As NAD^+ is used as a cell treatment, its possible interference with the assay was assessed. Contamination of the extracellular NAD^+ was tested and it was confirmed that >3 times washing with warm basal medium (DMEM) eliminates 3 mM NAD^+. For the ATP measurement, whether NAD^+ interferes with the assay was tested by spiking ATP standards with 400 nM NAD^+, and it was concluded that there is no interference by the compound. Furthermore, whether NAD^+ treatment could increase the ATP signal in the assay was tested by measuring a dose range of NAD^+ compound ATP levels, and concluded that NAD^+ did not introduce a false-positive signal. Also, the interference by the other compounds with the NAD^+ measurement was tested by spiking NAD^+ standards with 1 mM AMP, adenosine, guanosine, or uridine, and no cross-reaction was observed.

2.7. Metabolomics

Fibroblasts were detached by trypsinization and seeded at 14.000 cells/cm^2 to T25 cell culture flasks (#156367, Thermo Fisher Scientific). Treatments were performed as already described. Patient cells were treated with 1 mM compounds, except for NAD^+ precursors. Patient cells were treated with 10 mM NR or 3 mM NMN as they increased the intracellular NAD^+ levels comparable to 1 mM NAD^+ treatment. As NA and NAM did not increase NAD^+ levels, the highest non-toxic concentration (10 mM and 3 mM, respectively) under this study condition were used. Cells were harvested 24 h post-treatment by trypsinization followed by 5 min centrifugation at 400*g* at 4°C. The cell pellet was resuspended in 1 mL PBS, and 100 μL (1,10) of the cell suspension was separated into a different tubes for protein content determination. Samples for metabolomics and protein determination were centrifuged at 4200*g* for 3 min at 4°C. Supernatant was removed, and the cell pellet was washed with 1 mL PBS, followed by 3 min centrifugation at 4200*g* at 4°C. Supernatant was removed as much as possible and samples were snap-frozen in liquid nitrogen and stored at −80°C until the measurements. The metabolomics analysis was performed with liquid chromatography coupled to mass spectrometry (LC-MS) as described (Schomakers et al., 2022). Peak intensities of metabolites were corrected for internal standards and protein content.

Correlation analysis was performed using fold-change values of metabolites across all compound treatments (NAD^+, adenosine, AMP, NA, NAM, NR, NMN, pyruvate) in OXPHOS-reliant condition in patient cells. Fold changes were calculated by comparing OXPHOS-reliant condition with and without compound. For each metabolite, fold changes represent the mean of three independent experiments. Metabolites were excluded when not consistently detected in OXPHOS-reliant condition (i.e., absent in at least one replicate) (4 out of 72 metabolites).

2.8. Data analysis

Fluorescence microscopy images were analyzed using Image Pro Plus software (Media Cybernetics). OXPHOS viability experiments were included in the analysis only when the patient cells died after 72 h post treatment. Correlation and statistical analysis were performed using GraphPad PRISM software. The total number of independent experiments is marked with 'N', and the total number of technical replicates is marked with 'n'. Data in graphs represented as mean values of the independent experiments, and arrows indicate standard deviation.

Statistical significance was indicated in the figure legends for each experiment. **** $P < 0.0001$, *** $P < 0.001$, ** $P < 0.01$, * $P < 0.05$.

3. Results

3.1. Complex I-deficient patient fibroblasts do not survive in OXPHOS-reliant condition

Because Complex I-deficient patient fibroblasts grow relatively well in glucose-rich medium, we shifted them to galactose-containing medium to create an OXPHOS- reliant condition for our analyses. Under this condition, cellular viability was analyzed at 72 h post-treatment (Fig. 1a). No viability differences were observed between control and patient fibroblasts under control condition (glucose), whereas viability was significantly reduced in all four studied patient fibroblasts under OXPHOS-reliant condition, consistent with previous reports (Robinson et al., 1992; Iannetti et al., 2018) (Fig. 1b,c).

To confirm that the lack of Complex I activity was causative of the patient cells not surviving in the OXPHOS-reliant condition, two patient-derived fibroblast cell lines (PT3 and PT4), with mutations in the nuclear-encoded *NDUFS7* subunit of Complex I, and a control cell line, CT1, were transduced with the wild-type cDNA of the *NDUFS7* subunit.

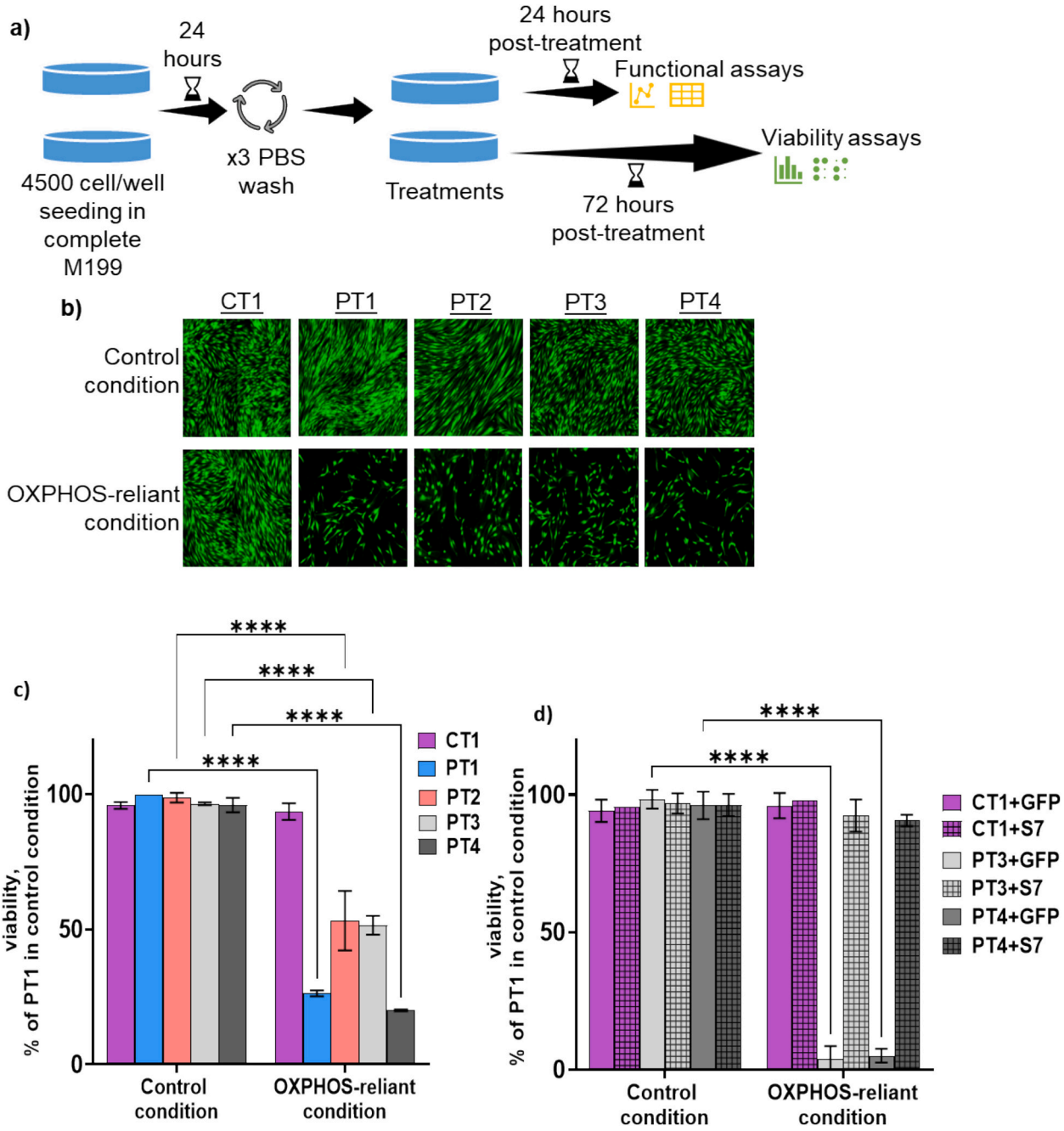


Fig. 1. Cell viability of control and Complex I-deficient patient fibroblasts in control versus OXPHOS-reliant condition a) Graphic representation of experimental workflow. b) Representative calcein-fluorescence microscopy images demonstrating cell viability at 72 h post-treatment of the patient and control cells in control versus OXPHOS-reliant condition. c) Quantification of cell viability of control and patient fibroblasts in control and OXPHOS-reliant conditions. ($N = 2$, $n = 12$ per cell line). Data are analyzed using 2-way ANOVA followed by Šídák's multiple comparisons test. d) Quantification of cell viability of the cell lines, either mock complemented (+GFP) or complemented with the wild-type S7 subunit (+S7), in control and OXPHOS-reliant conditions. ($N = 1$ $n = 2$ for CT1 + S7 cell line, $N = 3$ $n \geq 9$ for the rest of the cell lines. Data are analyzed using 2-way ANOVA followed by Šídák's multiple comparisons test.

The Complex I activity of the patient fibroblasts transduced with wild-type *NDUFS7* (PT3 + S7 and PT4 + S7) was increased compared to mock transductions (PT3 + GFP and PT4 + GFP), confirming the restoration of Complex I activity upon *NDUFS7* subunit complementation as reported by(Pecheritsyna et al., 2026). As expected, all fibroblast cell lines had a comparable viability in the control condition. In the OXPHOS-reliant condition, however, PT1 and mock-transduced patient fibroblasts had significantly decreased viability. The viability of the patient fibroblasts that were corrected with wild-type S7 subunit cDNA was rescued in OXPHOS-reliant condition (Fig. 1d). These results indicate that the Complex I deficiency is the underlying cause of the decreased cell viability of patient fibroblasts under the OXPHOS-reliant condition.

3.2. NAD^+ precursors do not improve patient cell viability or decrease lactate levels

Previously, direct NAD^+ treatment was shown to restore the viability of the Complex I-deficient primary fibroblasts to the level of control under OXPHOS-reliant condition(Iannetti et al., 2018). This finding prompted us to test whether NAD^+ precursors that have better bioavailability in in vitro and in vivo, such as NAM, NMN, NR, NA, and TG, could confer similar benefits. The cells selected for these experiments had intentionally very different residual Complex I activities (68% and 18% for PT1 and PT2, respectively).

In the control condition, both patient and control cells tolerated NAD^+ precursors well up to 3 mM, and toxicity was observed only at non-physiological concentrations as high as 10 mM for NAM, NMN, and NAD^+ (Fig. S2a-f). Cell viability of patient fibroblasts in OXPHOS-reliant condition was improved only upon treatment with NAD^+(Fig. 2). Also,

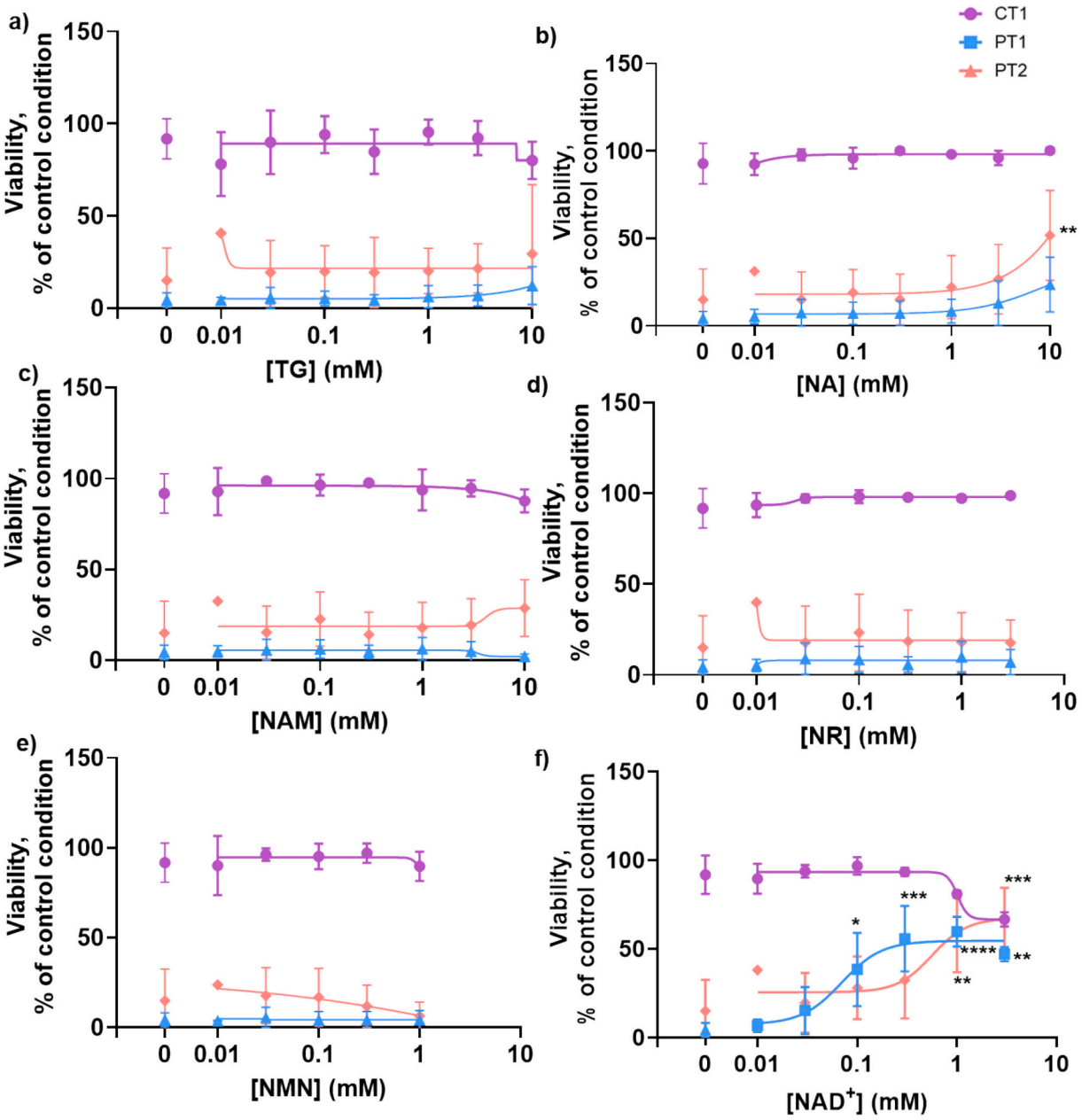


Fig. 2. Cell viability upon treatment with NAD^+ and NAD^+ precursors in OXPHOS-reliant condition. Quantification of cell viability of control and patient fibroblasts treated with a dose range of a) TG, b) NA, c) NAM, d) NR, e) NMN, and f) NAD^+ in OXPHOS-reliant condition. ($N \geq 3$, $n \geq 6$ per dose, per cell line). Data are analyzed using 2-way ANOVA followed by Dunnett's multiple comparisons test.

10 mM NA treatment significantly improved PT2 cell viability in OXPHOS-reliant condition, with a trend of viability improvement for PT1, however only at 10 mM which is a supraphysiological concentration (Fig. 2b). Since increased lactate production is considered a hallmark of PMD, lactate levels were quantified in the culture medium after 72-h treatment with NAD^+ and NAD^+ precursors in the control condition (Fig. S2g-l). NAD^+ treatment significantly decreased the extracellular lactate levels for both patient and control cell lines (Fig. S2l). Similar to the lack of effect on viability, NAD^+ precursors did not have a significant effect on extracellular lactate levels. We concluded that the NAD^+ precursors were not effective in rescuing the Complex I-deficient fibroblast in this model system, in contrast to NAD^+.

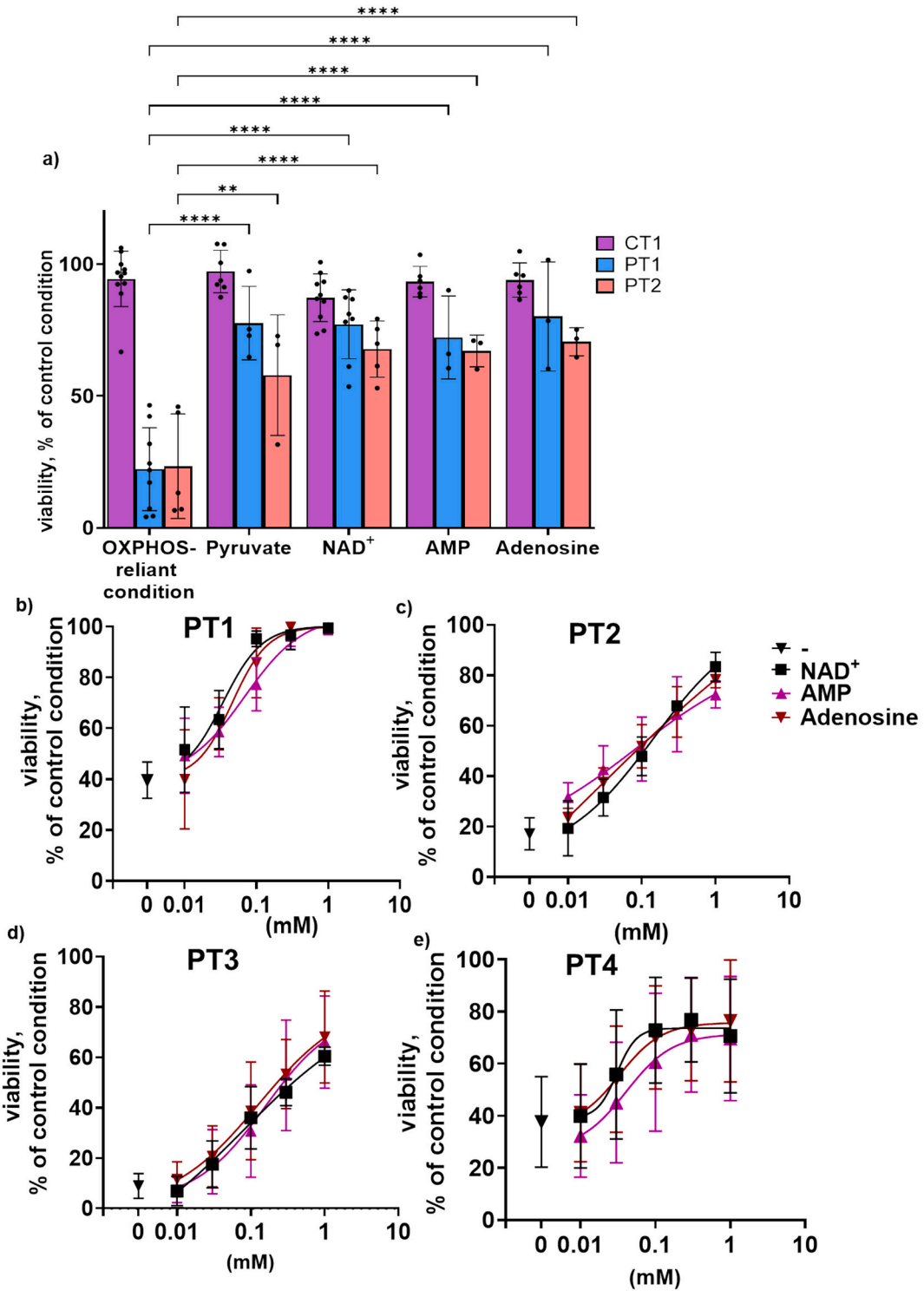


Fig. 3. Improved viability of patient fibroblasts upon treatment with NAD^+ and its structural moieties in OXPHOS-reliant condition a) Quantification of cell viability of control and patient fibroblasts in OXPHOS-reliant condition (vehicle) or supplementation with 1 mM Pyruvate, NAD^+, AMP, or adenosine in OXPHOS-reliant condition. Cell viability quantification of patient fibroblast b) PT1, c) PT2, d) PT3, e) PT4 in OXPHOS-reliant condition (−) with a dose range of NAD^+, AMP, or adenosine. ($N \geq 3$, $n \geq 6$). Data are analyzed using 2-way ANOVA followed by Dunnett's multiple comparison test.

3.3. Both NAD$^+$ and its structural components improve cell viability of the patient fibroblasts in OXPHOS-reliant condition

Since NAD$^+$ itself cannot directly enter the cells intact(Billington et al., 2008; Jie Zhang et al., 2018), we investigated whether its degradation products such as AMP and adenosine could account for the observed increase in viability. Control and patient fibroblasts were treated with AMP and adenosine under OXPHOS-reliant condition using pyruvate and NAD$^+$ as positive controls. The viability of the patient fibroblasts under OXPHOS-reliant condition was restored to control levels following treatment with 1 mM pyruvate, NAD$^+$, AMP, or adenosine (Fig. 3a). Treatment of the patient fibroblasts with a dose range of NAD$^+$, AMP, and adenosine under OXPHOS-reliant condition yielded comparable EC_{50} values of ~50–80 μM for all these compounds (Fig. 3b, c, d, e). This similarity suggests that these compounds may act via a similar mechanism to improve the patient fibroblast viability under OXPHOS-reliant condition.

3.4. Purine nucleosides promote survival of the patient fibroblasts under OXPHOS-reliant condition

Mitochondrial dysfunction is known to disrupt nucleotide metabolism (as reviewed in(MacVicar, 2025)). Since adenosine improved the cell viability of patient fibroblasts under OXPHOS-reliant condition, we next examined whether other purine and pyrimidine nucleosides produce similar effects. Control and patient fibroblasts were treated with different concentrations of guanosine, cytidine, and uridine under OXPHOS-reliant condition. Similar to adenosine (Fig. 3a, b), guanosine significantly improved patient fibroblast viability (Fig. 4a). Cytidine treatment had no effect (Fig. 4b), whereas uridine showed only a mild (10%) improvement in PT1 cell viability (Fig. 4c). Therefore, we conclude that purine, rather than pyrimidine, nucleosides confer the most robust cell viability benefit in patient cells under OXPHOS-reliant condition. Reduced glycolytic activity could limit the ribose availability. To test whether improved viability by purine nucleosides is mediated via ribose recycling (Fig. 4d), patient cells were treated with adenine, ribose, or adenosine under OXPHOS-reliant condition (Fig. 4e). Neither adenine base nor ribose treatment improved patient cell viability. This result indicates that improved patient cell viability under OXPHOS-reliant condition requires purine nucleoside metabolism and cannot be recapitulated by ribose or purine base supplementation alone.

3.5. No correlation between NAD$^+$ or ATP replenishment and improved cell viability in OXPHOS-reliant condition

Previous studies have shown that both NAD$^+$ and ATP levels can decrease under OXPHOS-reliant condition(Iannetti et al., 2018; Orlicka-Płocka et al., 2020; Dott et al., 2014). We, therefore, quantified intracellular NAD$^+$ or ATP levels in cells under this condition. Switching from control to OXPHOS-reliant condition did not alter intracellular NAD$^+$ or ATP levels for PT1 cells after 24-h treatment (102% of control condition), but both metabolites were markedly decreased in PT2 fibroblasts (62% of control condition), which have a low residual Complex I activity (Fig. 5a, b, S1). Treatment with NAD$^+$, NMN, and NR significantly increased intracellular NAD$^+$ levels for both cell lines, while TG, NA, and NAM had no effect (Fig. 5a). AMP and adenosine decreased NAD$^+$ levels in PT1, but not in PT2 cell line. Among all compounds, only NAD$^+$ treatment increased ATP levels in both patient fibroblast cell lines

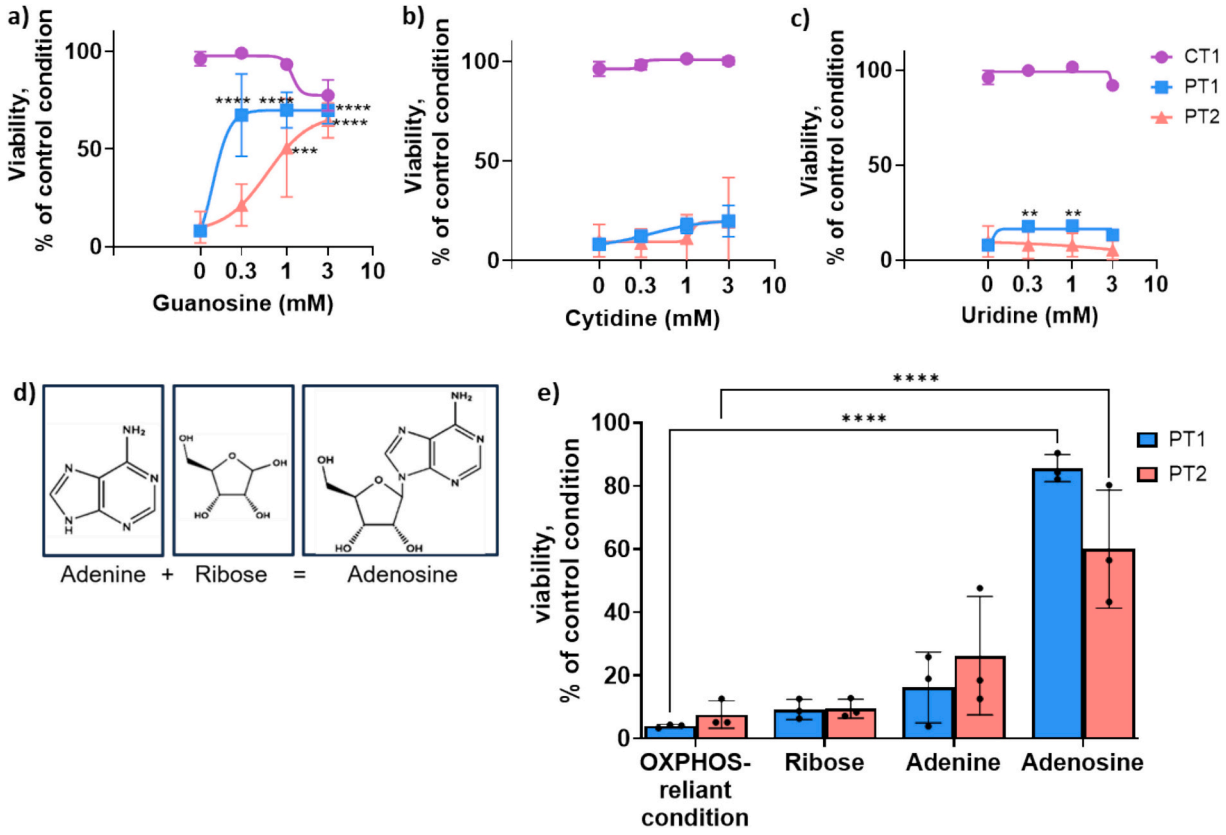


Fig. 4. Purine nucleoside treatment improved patient fibroblast viability in OXPHOS-reliant condition. Cell viability quantification of the control and patient fibroblasts in OXPHOS-reliant condition (x = 0), and a) 0.3–3 mM guanosine, b) 0.3–3 mM uridine, or c) 0.3–3 mM cytidine supplementation in OXPHOS-reliant condition. d) Chemical structure of adenine, ribose and adenosine. Created with MolView.org e) Quantification of cell viability of patient fibroblasts in OXPHOS-reliant condition or supplementation with 1 mM adenine, ribose, or adenosine in OXPHOS-reliant condition. ($N = 3$, $n \geq 6$). Data are analyzed using 2-way ANOVA followed by Dunnett's multiple comparison test.

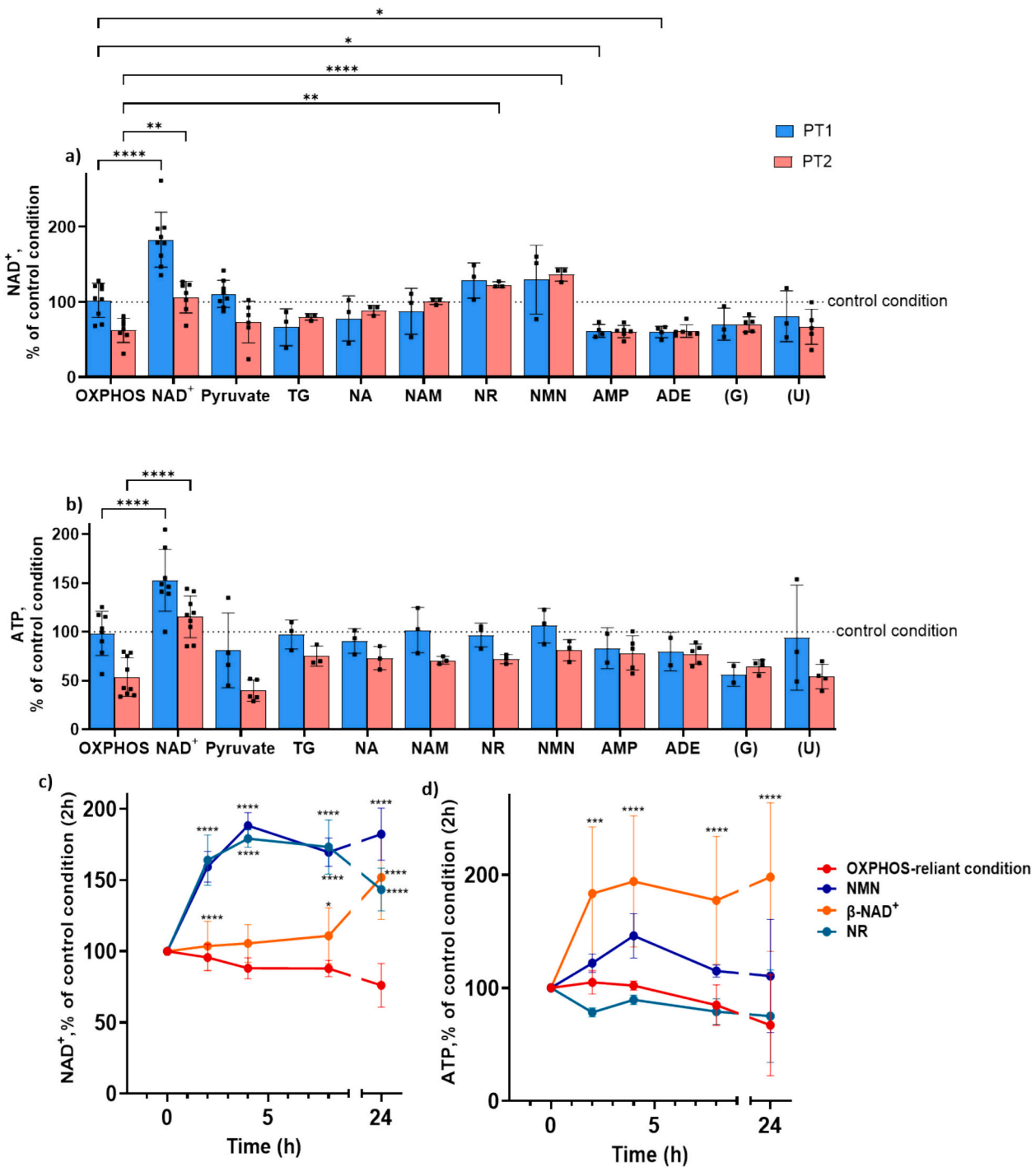


Fig. 5. Intracellular NAD^+ and ATP measurements upon compound treatment PT1 and PT2 fibroblasts were treated for 24 h in OXPHOS-reliant condition (indicated as OXPHOS) with the following treatments: 1 mM NAD^+, Pyruvate, TG, NA, NAM, NR, NMN, AMP, adenosine (A), guanosine (G), or uridine (U) in OXPHOS-reliant condition. A) Intracellular NAD^+ levels b) Intracellular ATP. ($N \geq 3$, $n \geq 9$ per cell line). Data are analyzed using 2-way ANOVA followed by Dunnett's multiple comparison test. Time course experiment with c) intracellular NAD^+ and d) ATP measurements of PT1 and PT2 fibroblasts in control condition, OXPHOS-reliant condition, or supplementation with 3 mM NMN, 10 mM NR, or 1 mM NAD^+ in OXPHOS-reliant condition ($N = 2$, $n = 4$ per cell line). Significance calculated compared to OXPHOS-reliant condition values at each time point, using 2-way ANOVA followed by Dunnett's multiple comparison test.

(Fig. 5b). All in all, changes in intracellular NAD^+ or ATP levels did not correlate with the viability rescue observed under the OXPHOS-reliant condition.

To assess the response over time on the levels of ATP and NAD^+, a time-course analysis was performed following treatment with NAD^+ and selected precursors (NR and NMN, both increasing NAD^+ levels 24 h post-treatment) (Fig. 5c). NAD^+ treatment with the dose of 1 mM marginally increased intracellular NAD^+ levels after 8 h under OXPHOS-reliant condition, with a more pronounced increase after 24 h (Fig. 5c). In contrast, this same treatment rapidly elevated intracellular ATP levels by 1.9-fold within 2 h (Fig. 5d). On the other hand, treatment with NMN and NR produced a much faster effect on NAD^+: both precursors increased intracellular NAD^+ levels by 1.7-fold within 2 h (Fig. 5c). NMN also induced a transient increase in intracellular ATP that returned

to the control levels at the 8-h time point (Fig. 5d). Together, these results indicate that under these conditions, NMN and NR act rapidly and are effective in boosting intracellular NAD^+ levels, whereas direct NAD^+ treatment more rapidly increases ATP levels. These distinct responses confirm that improved patient cell viability by NAD^+ treatment does not depend on increasing cellular NAD^+ levels.

3.6. Loss of Complex I activity impairs OXPHOS-dependent purine biosynthesis, as revealed by metabolic profiling

To gain more insight into the effect of the OXPHOS-reliant condition on cellular metabolism and to identify candidate metabolites promoting survival of patient cells, we performed a metabolomic analysis on cell extracts collected at 24 h post-treatment. A total of 72 metabolites were

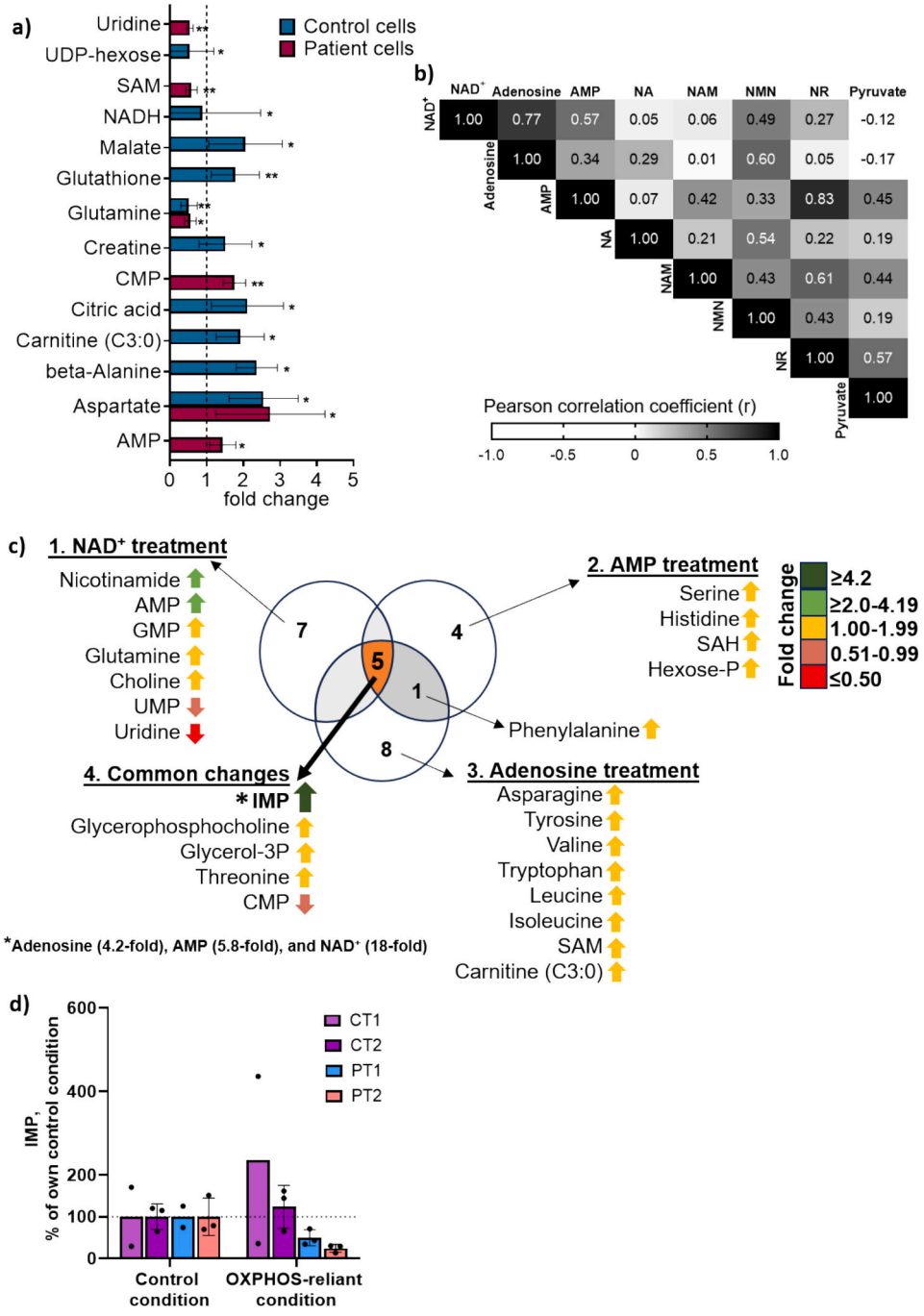


Fig. 6. Metabolomic LC-MS analysis of the control (CT1 and CT2) and patient (PT1 and PT2) fibroblasts upon 24 h post-treatment in different conditions. a) Fold change (paired *t*-test analysis) of the significantly changed ($P < 0.05$) metabolites upon switching from control to OXPHOS-reliant condition analyzed in control and patient fibroblasts. b) Pearson correlation matrix heatmap calculated using fold change of metabolites upon treatment with 1 mM NAD^+, 1 mM AMP, 1 mM adenosine (ADE), 10 mM NR, 10 mM NA, 3 mM NAM, 3 mM NMN, or 1 mM pyruvate compared to OXPHOS-reliant condition in patient fibroblasts. c) Venn diagram of the significantly changed metabolites (paired *t*-test analysis; $P < 0.05$) upon treatment with 1 mM NAD^+, ADE, or AMP in OXPHOS-reliant condition in the patient fibroblasts. ↑, increase in metabolite level; ↓, decrease in metabolite level. Metabolic analysis was performed on 3 biological repeats with 1 sample per cell line per condition. * indicates the fold change of IMP upon treatment with adenosine (4.2-fold), AMP (5.8-fold), or NAD^+ (18-fold) d) Bar graph of IMP levels in patient and control fibroblasts in control condition and OXPHOS-reliant condition, normalized to the average of control condition of each cell ($N \geq 2$, per cell line).

detected using LC-MS.

No metabolites were significantly different between control and patient fibroblasts in the control condition, indicating a similar metabolome when glucose is present in the culture condition (Fig. S3a). In contrast, switching from the control to the OXPHOS-reliant condition led to pronounced metabolic changes in both control and patient fibroblasts. In control cells, this shift produced the expected OXPHOS-associated response: increased levels of malate and citrate and decreased NADH levels(Liu et al., 2018; Singh et al., 2024) (Fig. 6a). This was not observed for the patient fibroblasts, but instead, the levels of monophosphorylated nucleotides, AMP and CMP, were slightly increased (Fig. 6a). In both patient and control fibroblasts, the OXPHOS-reliant condition induced a comparable increase in aspartate and decrease in glutamine levels, a pattern consistent with enhanced glutamate-dependent transamination, a pathway known to support proliferating cells(Alkan et al., 2018). In patient cells, uridine levels were decreased under OXPHOS-reliant condition without a significant change in UDP-hexose levels, whereas in control cells uridine diphosphate (UDP)-hexose levels were decreased. Thus, these findings indicate that while control fibroblasts show a typical OXPHOS driven metabolic shift, Complex I deficient patient cells engage distinct compensatory pathways, particularly within nucleotide metabolism, under mitochondrial stress.

The metabolic responses of the patient cells to the treatments under OXPHOS-reliant condition were then examined. Correlation analysis of mean fold changes for detected metabolites across all compound treatments, relative to OXPHOS-reliant condition, revealed several strong pairwise relationships (Fig. 6b). Among treatments that improve patient cell viability under OXPHOS-reliant condition, AMP and adenosine treatments showed high correlation with NAD^+ ($r > 0.5$), consistent with their structural association with NAD^+.

To identify which metabolites drive the viability enhancing effects of the treatments, we next examined the specific metabolite changes induced by NAD^+, AMP, and adenosine under OXPHOS-reliant conditions. AMP and adenosine treatment both moderately increased the branched-chain amino acids (valine, leucine, isoleucine), aromatic amino acids (phenylalanine, tyrosine, tryptophan), and one-carbon metabolism-related metabolites such as serine, S-Adenosylmethionine (SAM), and S-Adenosylhomocysteine (SAH). Across the metabolic profiles of the NAD^+, AMP, and adenosine treated cells, most significantly altered metabolites exhibited less than a 2-fold change (Fig. 6c). By contrast, inosine monophosphate (IMP), a critical intermediate in purine biosynthesis, showed a markedly larger increase, rising by 4.2-, 5.8-, and 18-fold following adenosine, AMP, or NAD^+ treatment, respectively. This pronounced elevation of IMP suggests that purine biosynthesis is a major metabolic pathway activated by these viability enhancing treatments under OXPHOS-reliant conditions.

We next examined whether basal IMP levels under OXPHOS stress could help explain the differential viability responses observed in patient versus control cells. In the control condition, IMP levels were highly variable, with patient cells showing a higher mean than control cells, although this difference was not statistically significant (Fig. 6d). Under OXPHOS-reliant conditions, however, IMP behaved distinctly in the two groups. In control cells, IMP levels increased relative to control condition (Fig. 6e) whereas in patient cells IMP levels were decreased by 50 and 75% for PT1 and PT2, respectively (Fig. 6e), indicating an impaired ability to maintain purine nucleotide pools during mitochondrial stress.

To determine whether non-purine viability-enhancing treatments acted through IMP-dependent or independent routes, we next examined NA and pyruvate. NA, which partially improved PT2 viability, showed mild (fold change <1.5) but significant ($P < 0.05$) changes in eight metabolites shown in Fig. S3b. Pyruvate, which improved the viability of both patient cells, increased intracellular lactate levels by 1.53-fold, potentially facilitating NAD^+ regeneration through NADH recycling (Fig. S3c). These responses occurred without major changes in IMP, indicating that pyruvate and NA support survival of patient fibroblasts through IMP-independent mechanisms.

Interestingly, the strongest overall correlation in metabolite changes occurred between AMP and NR treatment; however, only SAH was significantly increased by both AMP and NR (Fig. 6b-c, S3d). NMN and NR treatments increased IMP levels by 3.4-fold or less (Fig. S3e); yet neither of these treatments improved patient cell viability under the OXPHOS-reliant condition. This could indicate that a certain threshold for IMP elevation may be required for detectable viability benefit, but the IMP elevation alone is insufficient.

Taken together, these results show that OXPHOS-reliant condition is associated with decreased IMP levels in Complex I-deficient patient cells, and treatments rescuing viability, NAD^+, AMP, or adenosine, restore IMP levels. Therefore, these findings support a model in which viability enhancing effects of NAD^+, AMP and adenosine could be mediated through replenishment of IMP levels and activation of purine biosynthesis under OXPHOS-reliant condition.

4. Discussion

Previous research has shown that direct NAD^+ supplementation of Complex I-deficient cells in OXPHOS-reliant condition improves cell viability(Iannetti et al., 2018). Whether indirectly increasing the intracellular NAD^+ concentration by treatment with NAD^+ precursors, having more therapeutic potential than NAD^+ due to their better absorption and stability(Yusri et al., 2025), would have the same effect as NAD^+ in this condition was not previously tested.

NAD^+ precursors have shown metabolic benefits in some PMD in vitro models, such as NR-mediated rescue in NDUFS4-deficient iPSC-derived neurons primarily through increasing NAD^+ levels and activating sirtuin-dependent pathways(Yoon et al., 2022), while decreasing NADH levels in fibroblasts with a mitochondrial DNA mutation (m.3243 A > G)(Liufu et al., 2023). However, these effects have been demonstrated under standard glucose-rich conditions. In our OXPHOS-reliant setting, NAD^+ precursors such as NR and NMN increased NAD^+ levels, but they did not improve ATP levels or Complex I-deficient patient cell viability in the OXPHOS-reliant condition, or lactate accumulation. Only a slight improvement in patient cell viability was observed for NA, at a non-physiological 10 mM concentration in cell line PT2. Interestingly, we did not observe an increase in steady state NAD^+ or ATP levels upon NA treatment in our fibroblast model in OXPHOS-reliant condition. As direct NAD^+ treatment rapidly increases intracellular ATP levels and raises NAD^+ levels only at later time points while also improving viability, these results support a model in which early degradation of NAD^+ to AMP and adenosine could contribute to adenylated molecule pools first, and an increase in NAD^+ occurs later. NR, NMN, and NA lack this effect, possibly partially explaining their failure to rescue viability with physiological concentrations. Therefore, there is no direct correlation between improved cell viability and the ability of the compounds to modulate intracellular NAD^+ and/or ATP levels.

Mitochondrial dysfunction disturbs purine metabolism by depleting respiratory-dependent precursors like aspartate, inhibiting de novo synthesis through the accumulation of inhibitory intermediates like fumarate, and disrupting specialized transport and salvage enzymes that are essential for maintaining balanced nucleotide pools for both mitochondrial and nuclear genome stability(MacVicar, 2025). The most

striking compound treatment effect on metabolites was the increase in IMP levels by NAD^+, AMP, and adenosine, suggesting purine nucleotide metabolism as the target pathway in the OXPHOS-reliant condition. NR and NMN elevated IMP only mildly, and NA had no effect on IMP levels, aligning with their limited or absent impact on patient cell viability. This could indicate a threshold for IMP level to show viability improvement effect in OXPHOS-reliant condition. The high similarity in metabolic signatures produced by NAD^+, AMP, and adenosine indicates a similar mode of action of these compounds involving purine replenishment, whereas NAD^+ precursors primarily boost NAD^+ itself without meaningfully supporting the purine pool. Our findings are consistent with a report showing that inosine (the nucleoside part of IMP) supplementation restores the viability of galactosemia patient cells, which are unable to grow in galactose-containing media due to a deficiency in the galactose-1-phosphate uridyltransferase enzyme that metabolizes galactose in Leloir pathway(Pourci et al., 1990). Together, these observations support a model in which viability rescue under the OXPHOS-reliant condition requires restoration of purine intermediates, particularly IMP. The fact that treatment with ribose or the adenine purine base alone failed to improve the patient cell viability suggests that cellular energy status is insufficient to meet the energy demands of de novo purine biosynthesis pathway to restore IMP levels under OXPHOS-reliant condition, which makes the cells entirely dependent on the salvage pathway that is more rapid and energetically efficient.

As summarized in Fig. 7, it is proposed that under normal conditions, Complex I-deficient skin fibroblast cells rely on purine salvage into IMP and benefit from rapid ATP synthesis via glycolysis. OXPHOS-reliant condition makes both de novo synthesis and the salvage pathway difficult to sustain. Treatment with NAD^+, AMP, and adenosine could bypass these synthesis steps, decrease dependency on recycling, for example triphosphates (such as ATP), helping cells to stabilize IMP levels which are, as shown here, decreased in OXPHOS-reliant condition in patient cells. Whether exogenous NAD^+, AMP, and adenosine are directly converted to IMP in cells, via adenosine to inosine transformation, is not answered in the current study and will be further explored. While our study identifies significant alterations in purine metabolism under OXPHOS-reliant conditions, direct assessment of metabolic flux using isotope tracing would further refine understanding of purine metabolism.

An important limitation of this study is that the findings were obtained in patient-derived fibroblasts cultured under OXPHOS-reliant condition. Although this is an established in vitro strategy for exposing cellular vulnerabilities, it does not provide information regarding the systemic purine metabolism occurring in vivo. Thus, purine metabolism should currently be considered as a candidate metabolic vulnerability rather than a validated therapeutic target. Future studies should first determine whether the purine alterations identified in this study are reproduced in relevant in vivo Complex I-deficiency models, such as Ndufs4-deficient mice, before assessing the effects of pharmacological intervention.

5. Conclusions

This study highlights purine metabolism as the bottleneck of survival of Complex I-deficient fibroblasts in OXPHOS-reliant conditions. Improved patient cell survival by NAD^+ and AMP is mediated via adenosine by increasing IMP levels, which in turn can balance AMP and ATP turnover. Furthermore, this study provides new mechanistic

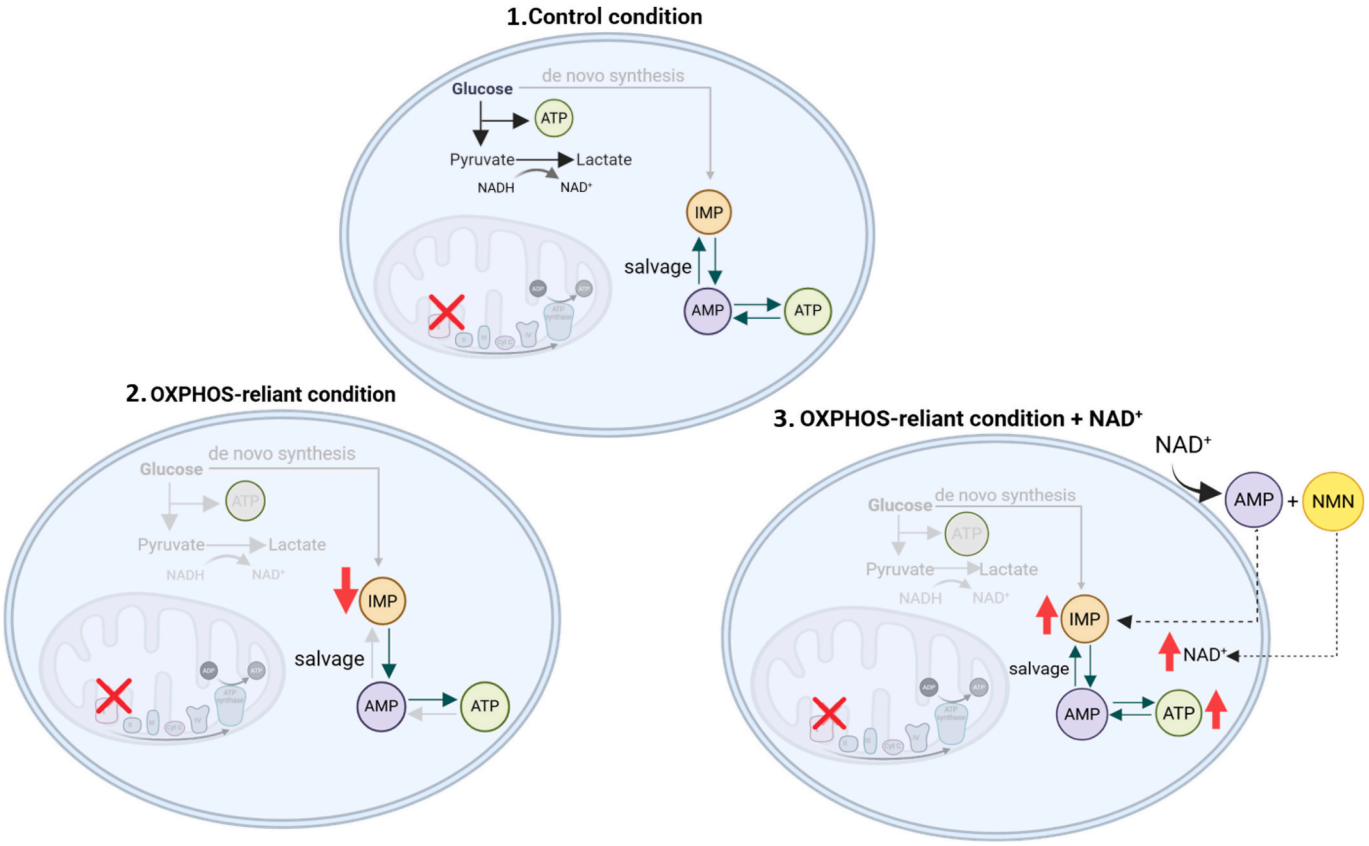


Fig. 7. Illustration of the proposed mechanism of NAD^+-mediated improved viability of Complex I-deficient patient cells. OXPHOS impairment makes cells rely on the purine salvage pathway. Rapid ATP synthesis and NADH recycling via glycolysis compensates purine salvage under control condition. OXPHOS-reliant condition limits this rapid ATP turnover and alter redox state, which eventually leads to decreased purine precursor IMP levels. When supplemented in OXPHOS-reliant condition, degradation of NAD^+ into AMP increases intracellular IMP levels, which also restores ATP levels. NMN moiety is responsible for the increased NAD^+ levels subsequently. Created with BioRender.com

insights into the 'galactose assay', by establishing the purine metabolism dysfunction as the patient cell death-causing pathway. Our findings highlight purine metabolism as both a candidate therapeutic target for further in vivo testing and a basis for improving galactose assay-driven drug discovery strategies.

CRediT authorship contribution statement

Melisa Emel Ermert: Writing – review & editing, Writing – original draft, Visualization, Methodology, Investigation, Conceptualization. **Bas Pennings:** Methodology, Investigation. **Anja Perkovic:** Investigation. **Svetlana Pecheritsyna:** Writing – review & editing, Supervision, Methodology, Conceptualization. **Bauke Schomakers:** Writing – review & editing, Investigation. **Michel van Weeghel:** Writing – review & editing, Investigation. **Jan Smeitink:** Writing – review & editing, Supervision, Funding acquisition. **Riekelt Houtkooper:** Writing – review & editing, Supervision, Funding acquisition, Conceptualization. **Eija Pirinen:** Writing – review & editing, Supervision. **Herma Renkema:** Writing – review & editing, Writing – original draft, Validation, Supervision, Methodology, Conceptualization.

Funding

This project was financially supported by funding from the European Union's Horizon Europe research and innovation program through the NADIS project (no. 101073251; www.nadis.eu). E.P.; Research Council of Finland Profi6 funding (grant no 336449) awarded to the University of Oulu.

Declaration of competing interest

Jan Smeitink (Founder, Chairman of the Supervisory Board), Herma Renkema (CSO) and Bas Pennings are employees of Khondrion.

Acknowledgements

The authors are grateful to Professor Santina Bruzzone and other members of the NADIS consortium for their insightful discussions and recommendations regarding experiments in this study model.

Appendix A. Supplementary data

Supplementary data to this article can be found online at https://doi.org/10.1016/j.mito.2026.102223.

Data availability statement

The raw data supporting the conclusions of this article will be made available by the authors on request.

References

Adant, Isabelle, Bird, Matthew, Decru, Bram, Windmolders, Petra, Wallays, Marie, de Witte, Peter, Rymen, Daisy, et al., 2022. Pyruvate and uridine rescue the metabolic profile of OXPHOS dysfunction. Mol. Metab. 63, 101537. https://doi.org/10.1016/J.MOLMET.2022.101537.

Alkan, H. Furkan, Walter, Katharina E., Luengo, Alba, Madreiter-Sokolowski, Corina T., Stryeck, Sarah, Lau, Allison N., Al-Zoughbi, Wael, et al., 2018. Cytosolic aspartate availability determines cell survival when glutamine is limiting. Cell Metab. 28 (5), 706–720 e6. https://doi.org/10.1016/J.CMET.2018.07.021/ATTACHMENT/5B435859-BFE7-4C1F-8992-FC4FF4F77466/MMC2.PDF.

Billington, Richard A., Travelli, Cristina, Ercolano, Emanuela, Galli, Ubaldina, Roman, Cintia Blasi, Grolla, Ambra A., Canonico, Pier Luigi, Condorelli, Fabrizio, Genazzani, Armando A., 2008. Characterization of NAD uptake in mammalian cells. J. Biol. Chem. 283 (10), 6367–6374. https://doi.org/10.1074/jbc.M706204200.

Chinnery, Patrick F., 2021. Primary mitochondrial disorders overview. GeneReviews®, July. https://www.ncbi.nlm.nih.gov/books/NBK1224/.

Kok, Michèle J.C. de, Schaapherder, Alexander F., Wüst, Rob C.I., Zuiderwijk, Melissa, Bakker, Jaap A., Lindeman, Jan H.N., Le Dévédec, Sylvia E., 2021. Circumventing the Crabtree effect in cell culture: a systematic review. Mitochondrion 59, 83–95. https://doi.org/10.1016/J.MITO.2021.03.014.

Dott, William, Mistry, Pratibha, Wright, Jayne, Cain, Kelvin, Herbert, Karl E., 2014. Modulation of mitochondrial bioenergetics in a skeletal muscle cell line model of mitochondrial toxicity. Redox Biol. 2 (1), 224–233. https://doi.org/10.1016/J.REDOX.2013.12.028.

EPAR, 2015. EPAR,2015. https://www.ema.europa.eu/en/medicines/human/EPAR/raxone.

EPAR, 2026. EPAR,2026. https://www.ema.europa.eu/en/medicines/human/EPAR/kygevvi.

FDA, 2025. FDA,2025, 2025. https://www.fda.gov/news-events/press-announcements/fda-grants-accelerated-approval-first-treatment-barth-syndrome.

Iannetti, Eligio F., Smeitink, Jan A.M., Beyrath, Julien, Willems, Peter H.G.M., Koopman, Werner J.H., 2016. Multiplexed high-content analysis of mitochondrial morphofunction using live-cell microscopy. Nat. Protoc. 1693–1710. https://doi.org/10.1038/nprot.2016.094, 11:9.

Iannetti, Eligio F., Smeitink, Jan A.M., Willems, Peter H.G.M., Beyrath, Julien, Koopman, Werner J.H., 2018. Rescue from galactose-induced death of Leigh syndrome patient cells by pyruvate and NAD+. Cell Death Dis. 9 (11). https://doi.org/10.1038/S41419-018-1179-4.

Imai, Shin ichiro, Johnson, Sean, 2018. NAD+ biosynthesis, aging, and disease. F1000Res 7, 1–10. https://doi.org/10.12688/f1000research.12120.1.

Koopman, Werner J.H., Verkaart, Sjoerd, Visch, Henk Jan, Van Emst-De Vries, Sjenet, Nijtmans, Leo G.J., Smeitink, Jan A.M., Willems, Peter H.G.M., 2007. Human NADH: ubiquinone oxidoreductase deficiency: radical changes in mitochondrial morphology?, 293, pp. 22–29. https://doi.org/10.1152/Ajpcell.00194.2006, 1.

Liu, Ling, Su, Xiaoyang, Quinn, William J., Hui, Sheng, Krukenberg, Kristin, Frederick, David W., Redpath, Philip, et al., 2018. Quantitative analysis of NAD synthesis-breakdown fluxes. Cell Metab. 27 (5), 1067–1080.e5. https://doi.org/10.1016/j.cmet.2018.03.018.

Liufu, Tongling, Yu, Haiyan, Yu, Jiaxi, Yu, Meng, Tian, Yue, Ou, Yichun, Deng, Jianwen, Xing, Guogang, Wang, Zhaoxia, 2023. Complex I deficiency in m.3243A>G fibroblasts is alleviated by reducing NADH accumulation. Front. Physiol. 14, 1164287. https://doi.org/10.3389/FPHYS.2023.1164287/TEXT.

MacVicar, Thomas, 2025. High tide or low tide: the transport and metabolism of mitochondrial nucleotides. Biochem. J. 482 (16), 1144–1161. https://doi.org/10.1042/BCJ20253237.

Membrez, Mathieu, Migliavacca, Eugenia, Christen, Stefan, Yaku, Keisuke, Trieu, Jennifer, Lee, Alaina K., Morandini, Francesco, et al., 2024. Trigonelline is an NAD+ precursor that improves muscle function during ageing and is reduced in human sarcopenia. Nat. Metab. 6 (3), 433–447. https://doi.org/10.1038/S42255-024-00997-X;SUBJMETA.

Nakamura, Michinari, Bhatnagar, Aruni, Sadoshima, Junichi, 2012. Overview to pyridine nucleotides review series. Circ. Res. 111 (5), 604. https://doi.org/10.1161/CIRCRESAHA.111.247924.

Orlicka-Płocka, Marta, Gurda-Wozna, Dorota, Fedoruk-Wyszomirska, Agnieszka, Wyszko, Eliza, 2020. Circumventing the Crabtree effect: forcing oxidative phosphorylation (OXPHOS) via galactose medium increases sensitivity of HepG2 cells to the purine derivative kinetin riboside. Apoptosis 25 (11−12), 835–852. https://doi.org/10.1007/S10495-020-01637-X/FIGURES/5.

Pecheritsyna, Svetlana, Ermert, Melisa Emel, Podhumljak, Emina, Pennings, Bas, Zondag, Ruth, Iannetti, Eligio F., Renkema, Herma, Smeitink, Jan, 2026. Sensitivity of primary mitochondrial disease fibroblasts to ferroptosis: the role of intracellular iron. Mitochondrion 87, 102112. https://doi.org/10.1016/J.MITO.2026.102112.

Pourci, M.L., Mangeot, M., Soni, T., Lemonnier, A., 1990. Culture of galactosaemic fibroblasts in the presence of galactose: effect of inosine. J. Inherit. Metab. Dis. 13 (6), 819–828. https://doi.org/10.1007/BF01800205.

Renkema, G. Herma, Wortmann, Saskia B., Smeets, Roel J., Venselaar, Hanka, Antoine, Marion, Visser, Gepke, Ben-Omran, Tawfeg, et al., 2014. SDHA mutations causing a multisystem mitochondrial disease: novel mutations and genetic overlap with hereditary tumors. Eur. J. Hum. Genet. 23 (2), 202. https://doi.org/10.1038/EJHG.2014.80.

Robinson, B.H., Petrova-Benedict, R., Buncic, J.R., Wallace, D.C., 1992. Nonviability of cells with oxidative defects in galactose medium: A screening test for affected patient fibroblasts. Biochem. Med. Metab. Biol. 48 (2), 122–126. https://doi.org/10.1016/0885-4505(92)90056-5.

Schmiedeknecht, Kira, Kaufmann, Andreas, Bauer, Stefan, Venegas Solis, Francisco, 2022. L-lactate as an indicator for cellular metabolic status: an easy and cost-effective colorimetric L-lactate assay. PLoS One 17 (7), e0271818. https://doi.org/10.1371/JOURNAL.PONE.0271818.

Schomakers, Bauke V., Hermans, Jill, Jaspers, Yorrick R.J., Salomons, Gajja, Vaz, Frédéric M., van Weeghel, Michel, Houtkooper, Riekelt H., 2022. Polar metabolomics in human muscle biopsies using a liquid-liquid extraction and Full-scan LC-MS. STAR Protocols 3 (2). https://doi.org/10.1016/J.XPRO.2022.101302.

Singh, Rita, Fatima, Eram, Thakur, Lovnish, Singh, Sevaram, Ratan, Chandra, Kumar, Niraj, 2024. Advancements in CHO metabolomics: techniques, current state and evolving methodologies. Front. Bioeng. Biotechnol. 12, 1347138. https://doi.org/10.3389/FBIOE.2024.1347138/FULL.

Xiao, Wusheng, Loscalzo, Joseph, 2020. Metabolic responses to reductive stress. Antioxid. Redox Signal. 32 (18), 1330–1347. https://doi.org/10.1089/ARS.2019.7803/ASSET/IMAGES/ARS.2019.7803_FIGURE8.JPG.

Yoon, Jin-Young, Daneshgar, Nastaran, Chu, Yi, Chen, Biyi, Hefti, Marco, Vikram, Ajit, Irani, Kaikobad, et al., 2022. Metabolic rescue ameliorates mitochondrial Encephalocardiomyopathy in murine and human IPSC models of Leigh syndrome. Clin. Transl. Med. 12 (7). https://doi.org/10.1002/ctm2.954.

Yusri, Khalishah, Jose, Sandra, Vermeulen, Karen S., Tan, Trina Chia Min, Sorrentino, Vincenzo, 2025. The role of NAD+ metabolism and its modulation of mitochondria in aging and disease. NPJ Metabolic Health and Disease 3 (1). https://doi.org/10.1038/s44324-025-00067-0.

Zhang, Jie, Wang, Caixia, Shi, Haibo, Wu, Danhong, Ying, Weihai, 2018. Extracellular degradation into adenosine and the activities of adenosine kinase and AMPK mediate extracellular NAD+-produced increases in the adenylate pool of BV2 microglia under basal conditions. Front. Cell. Neurosci. 12, 343. https://doi.org/10.3389/FNCEL.2018.00343/FULL.

Zhang, Jianying, Wang, He Ling, Lautrup, Sofie, Nilsen, Hilde Loge, Treebak, Jonas T., Watne, Leiv Otto, Selbæk, Geir, et al., 2025. Emerging strategies, applications and challenges of targeting NAD+ in the clinic. Nat. Aging 5 (9), 1704–1731. https://doi.org/10.1038/s43587-025-00947-6.

Zong, Yao, Li, Hao, Liao, Peng, Chen, Long, Pan, Yao, Zheng, Yongqiang, Zhang, Changqing, Liu, Delin, Zheng, Minghao, Gao, Junjie, 2024. Mitochondrial dysfunction: mechanisms and advances in therapy. Signal Transduct. Target. Ther. 9 (1), 1–29. https://doi.org/10.1038/s41392-024-01839-8.